IMPLICIT INTEGRATION ALGORITHM FOR HOEK-BROWN ELASTIC-PLASTIC MODEL

RICHARD G. WAN

MRL 93-004(J) April 1993

Published in Computers and Geotechnics 14 (1992) 149-177

IMPLICIT INTEGRATION ALGORITHM FOR HOEK-BROWN ELASTIC-PLASTIC MODEL

R. G. WAN
Canada Centre for Mineral and Energy Technology
Mining Research Laboratories, Ottawa, K1A 0G1, Canada

ABSTRACT

A realistic strength criterion often used to describe the yielding behaviour of a jointed rock mass at a continuum level is the well-known Hoek and Brown criterion. This paper is concerned with a 3-D stress generalization of the Hoek-Brown failure criterion by means of an elliptical functional which leads to a smooth deviatoric trace in the stress space. For its incorporation into a finite element analysis involving plasticity calculations, the formulation of an implicit stress integration algorithm is presented. The key computational methodology alludes to the notion of consistent tangent modulus and implicit return mapping schemes (radial and closest point return) for stress integration in a finite element analysis. Within the context of non-linear elastoplastic analysis, it is found that formulation of such consistent modulus and success into achieving numerical efficiency are closely intertwined. Indeed, the procedure results into accurate and rapid convergence of the displacement finite element scheme during the search for equilibrium. This means that considerable savings in computational time can be achieved for large scale problems. Numerical examples which focus on the Hoek-Brown plasticity model are presented in order to fully appreciate the robustness of the algorithm, and hence the viability of such method to practical problems.

INTRODUCTION

Constitutive models find their usefulness when they are used in conjunction with the finite element method to describe material behaviour in a general boundary value problem setting. For modelling rocks, the Hoek-Brown failure criterion has been widely used to characterize strength of material from both laboratory and site data. However, rarely has it been regarded as a yield surface and integrated into the theory of plasticity to compute strains

and displacements in the yielded rock via finite elements. Coupled with the empirical nature of the Hoek-Brown failure criterion, numerical breakdowns in the severe stress regimes have in general impeded its application to elastoplastic solutions of equivalent continuum rock masses.

This paper focuses on the generic problem of constitutive stress integration in the context of elastoplastic calculations. The computational structure of a finite element analysis which involves non-linear material behaviour comprises two major aspects. First, the equilibrium corrector must ensure that the integrated stress state and the associated plasticity state variables (hardening/softening parameters) conform with the yield condition, i.e. full consistency conditions must be met at discrete stages of the solution process. Second, the solution of non-linear equations of equilibrium must be consistently linearized in conjunction with the integrated stress, a point which is very often overlooked at the detriment of accurate numerical computations.

The key issue of the present discussion arises in the case of large excavations for example, when the load increment is no longer infinitesimal in order to justify the approximations made during linearization of the finite element equations. The approach chosen to integrate the constitutive law then becomes a crucial factor for achieving numerical accuracy and stability. Several explicit and implicit integration schemes are being used for elastoplastic computations. On the one hand, explicit integration usually requires the determination of the elastic-elastoplastic transition through the calculation of a contact stress on the yield surface and a scaling factor for the plastic multiplier, see Owen & Hinton [1]. At some times, in cases of complex stress and loading conditions, this procedure breaks down and can produce undesirable phenomena such as negative plastic flow, a case when the plastic multiplier numerically becomes negative, as reported in Deng & Rosakis [2]. Also, it is computationally inefficient especially for complex yield surfaces that require an iterative procedure for finding the scaling factor and contact stresses on the yield surface. On the other hand, implicit methods—of which the predictor/corrector scheme forms part—are more accurate and numerically robust for cases of finite loads. This class of numerical algorithm originates from the work of Wilkins [3] for the radial return in J_2 plasticity analysis, and has been investigated in various contexts. An example is the establishment of the notion of closest point return for the overstress, see [4,5,6].

Just as important as the stress integration scheme, is the linearization of the equilibrium equations which arise from a finite element idealization. It is found that in most instances, linearization of the equilibrium equations is carried out independently of the stress integration method adopted for the constitutive law. Consequently, the elastoplastic modulus commonly used in deriving the tangent stiffness matrix is inconsistent with the

stress integration scheme. Very often, the approximation which results from such calculations leads to degradation of convergency characteristics of the problem. While this deterioration appears to be insignificant for simple constitutive models, it can be prominent for highly non-linear situations involving truly finite loads and complex material behaviour.

In this paper, a so-called algorithmic tangent moduli, as coined by Simo & Hughes [6], is derived for a plasticity model based on a form of 3-D Hoek-Brown failure criterion with associated and non-associated flow rules. The solution of the discrete problem is obtained incrementally using a full Newton method in conjunction with an exact linearized consistent tangent modulus. The procedure includes an initial elastic step followed by an elastoplastic correction step which ensures the exact satisfaction of the plastic consistency condition by solving locally a scalar non-linear equation in addition to the global equilibrium equations. The other salient feature is the expression of a consistent (algorithmic) elastoplastic tangent stiffness in a form which is computationally attractive. For tension, a cut-off surface is used and special attention is given to the singular corner region formed at the intersection of the 3-D Hoek-Brown and the tension cut-off surfaces. As such, when the elastic predictor falls in the tensile zone, a consistent stress return is enforced. It is found that due to its consistency with the notion of closest point mapping, this stress return avoids notorious numerical breakdowns in such tensile stress situations, and consequently rapid equilibrium convergence is conserved.

PRELIMINARIES

Consider the standard displacement type finite element setting in which the incremental displacement and resulting strain fields are usually given. The aim is to solve the continuum elastoplastic problem incrementally by computing the actual stress-strain response function during the search for global equilibrium. The discrete algorithmic problem for the simple case of perfect plasticity can be stated as follows: given the stress, total and plastic strain fields at pseudo-time t_n, compute new states at final pseudo-time t_{n+1}, i.e.

$$\left\{\boldsymbol{\sigma}_n, \boldsymbol{\varepsilon}_n, \boldsymbol{\varepsilon}_n^p\right\} \rightarrow \left\{\boldsymbol{\sigma}_{n+1}, \boldsymbol{\varepsilon}_{n+1}, \boldsymbol{\varepsilon}_{n+1}^p\right\}. \tag{1}$$

Concurrently, incremental equilibrium must be fulfilled by requiring

$$\int_\Omega \boldsymbol{\sigma}_{n+1} : \Delta\boldsymbol{\varepsilon}_{n+1}\, d\Omega = \int_\Omega \mathbf{f} : \Delta\mathbf{u}_{n+1}\, d\Omega + \int_\Gamma \mathbf{T} : \Delta\mathbf{u}_{n+1}\, d\Gamma, \tag{2}$$

where **f** and **T** are the body and traction forces respectively, Ω the volume of interest and Γ the boundary along which tractions are applied. Generally speaking, the key incremental variables can be typically calculated by invoking the kinematic conditions, the additivity of elastic and plastic strain increments and the flow rule of plasticity as:

$$\Delta\boldsymbol{\varepsilon}_{n+1} = \mathbf{B}:\Delta\mathbf{u}_{n+1}; \Delta\boldsymbol{\sigma}_{n+1} = \mathbf{C}^e:(\Delta\boldsymbol{\varepsilon}_{n+1} - \Delta\boldsymbol{\varepsilon}^p_{n+1}); \Delta\boldsymbol{\varepsilon}^p_{n+1} = \Delta\lambda_{n+1}\,\partial_\sigma Q_{n+1}, \tag{3}$$

in which **B** is the strain-displacement operator, $\mathbf{C}^e$ the elastic tensor, λ the plastic multiplier, Q the plastic potential and ∂_σ the gradient operator. Accordingly, it is possible to recast the elastoplastic problem into an evolution problem where the final stress $\boldsymbol{\sigma}_{n+1}$ must lie on the yield surface F, i.e.

$$\boldsymbol{\sigma}_{n+1} = \mathbf{C}^e:(\boldsymbol{\varepsilon}_{n+1} - \boldsymbol{\varepsilon}^p_{n+1}), \quad \boldsymbol{\varepsilon}^p_{n+1} = \boldsymbol{\varepsilon}^p_n + \lambda_{n+1}\,\partial_\sigma Q_{n+1}, \quad F(\boldsymbol{\sigma}_{n+1}) \equiv 0. \tag{4}$$

From the above (Eqs. 4a,b), the final stress $\boldsymbol{\sigma}_{n+1}$ can be rewritten conveniently as

$$\boldsymbol{\sigma}_{n+1} = \boldsymbol{\sigma}^{tr}_{n+1} - \lambda_{n+1}\,\mathbf{C}^e:\partial_\sigma Q_{n+1}, \tag{5}$$

which can be interpreted as the projection of the trial stress (elastic predictor) onto the yield surface. When the yield function F coincides with the plastic potential Q, the transformation which results from such projection is indeed the closest point projection due to the convexity of the functions. The plastic multiplier which gives the magnitude of the stress projection is obtained by linearizing Eq. (4c) about the final stress in an implicit fashion. This procedure when combined with the linearization of Eq. (2) gives rise to the calculation of the so called consistent tangent operator which is different from the classical elastoplastic (continuum) tangent operator in many aspects, see Willam [7].

CONSISTENT LINEARIZATION OF FINITE ELEMENT EQUATIONS

The linearization of Eq. 2 reduces to equilibrating internal forces $\mathbf{F}_{int}$ with external forces $\mathbf{F}_{ext}$. The internal force which refers to equivalent forces resulting from a given stress field $\boldsymbol{\sigma}$ is expressed as:

$$\mathbf{F}_{int} = \int_\Omega \mathbf{B}^{\mathrm{T}}:\boldsymbol{\sigma}_{n+1}\, d\Omega. \tag{6}$$

Consider that one wishes to advance the solution from pseudo time station t_n where principal variables $\mathbf{u}_n$, $\boldsymbol{\varepsilon}_n$, $\boldsymbol{\sigma}_n$ are known, to t_{n+1}. Since equilibrium has to be established also at t_{n+1} for a new displacement field $\mathbf{u}_{n+1}$, ideally,

$$\mathbf{F}_{int}(\mathbf{u}_{n+1}) = \mathbf{F}_{ext}. \tag{7}$$

Here, the expression of $\mathbf{F}_{int}$ depends on the final stresses, strains and displacements which are in fact unknown; hence the solution has to be iteratively found from

$$\mathbf{F}_{int}(\mathbf{u}^k_{n+1} + \Delta\mathbf{u}^k_{n+1}) = \mathbf{F}_{ext}, \tag{8}$$

where k corresponds to the kth. iteration during successive attempts to find the final displacement $\mathbf{u}_{n+1}$. Expanding the above into a Taylor's series around $n+1$ at the kth. iteration and keeping only first order terms results into:

$$\begin{aligned}
&\mathbf{F}_{\text{int}}(\mathbf{u}^k_{n+1}) + \left.\frac{\partial \mathbf{F}_{\text{int}}}{\partial \mathbf{u}}\right|^k_{n+1} \Delta\mathbf{u}^k_{n+1} + O(\Delta\mathbf{u}^2_{n+1}) = \mathbf{F}_{ext}, \\
&\Delta\mathbf{u}^k_{n+1} = \left[\mathbf{J}^k_{n+1}\right]^{-1}\left(\mathbf{F}_{ext} - \mathbf{F}_{\text{int}}(\mathbf{u}^k_{n+1})\right), \\
&\left[\mathbf{J}^k_{n+1}\right]^{-1} = \left.\frac{\partial \mathbf{F}_{\text{int}}}{\partial \mathbf{u}}\right|^k_{n+1}.
\end{aligned} \tag{9}$$

Based on Eq. 9b from which corrective displacements are calculated, the displacement at the end of the kth. attempt simply becomes

$$\mathbf{u}^{k+1}_{n+1} = \mathbf{u}^k_n + \Delta\mathbf{u}^k_{n+1}. \tag{10}$$

In a classical fashion, successive iterates are performed until the internal force $\mathbf{F}_{int}$ equals to the external force $\mathbf{F}_{ext}$ within a certain tolerance.

Calculation of Jacobian J

The Jacobian **J**, Eq. 9c, which emerges from linearizing the equilibrium equations reflects the variation of each component of the internal forces given in Eq. 6 with each component of the displacements. Thus, for the kth. iteration, one gets

$$\mathbf{J}^k_{n+1} = \frac{\partial \mathbf{F}_{\text{int}}}{\partial \mathbf{u}^k_{n+1}} = \int_\Omega \mathbf{B}^T : \frac{\partial \boldsymbol{\sigma}^k_{n+1}}{\partial \mathbf{u}^k_{n+1}} \, d\Omega. \tag{11}$$

Further differentiation gives

$$\frac{\partial \boldsymbol{\sigma}^k_{n+1}}{\partial \mathbf{u}^k_{n+1}} = \frac{\partial \boldsymbol{\sigma}^k_{n+1}}{\partial \boldsymbol{\varepsilon}^k_{n+1}} : \frac{\partial \boldsymbol{\varepsilon}^k_{n+1}}{\partial \mathbf{u}^k_{n+1}} = \frac{\partial \boldsymbol{\sigma}^k_{n+1}}{\partial \boldsymbol{\varepsilon}^k_{n+1}} : \mathbf{B}^T. \tag{12}$$

When the above is substituted into Eq. 11, the expression of the Jacobian matrix takes a more recognizable form:

$$\mathbf{J}^k_{n+1} = \int_\Omega \mathbf{B}^T : \mathbf{C}^k_{n+1} : \mathbf{B} \; d\Omega, \quad \mathbf{C}^k_{n+1} = \frac{\partial \boldsymbol{\sigma}^k_{n+1}}{\partial \boldsymbol{\varepsilon}^k_{n+1}}. \tag{13}$$

It is found that the rate of convergence of the equilibrium Newton-Raphson scheme depends critically on the correct evaluation of the Jacobian J. Equation 13 is central for the calculation of the so called consistent modulus which relies on the expression of the incremental stress-strain relationship in a stress return fashion, Eq. 5. The developments in subsequent sections focusses on the derivation of such a consistent tangent modulus for the Hoek-Brown failure/yield criterion commonly used in rock problems. Applications to soil problems such as in the integration of Cam-clay type of models have been very successful, see Borja [8].

ROCK PLASTICITY

An important phenomenon manifested by rock strata in the vicinity of rock openings is their non-linear behaviour in response to induced stress. This non-linearity can often be attributed to the formation, closure or opening of cracks. For the mathematical description of the non-linear behaviour of the rock mass, a yield criterion based on the theory of plasticity is needed.

In order to determine the yielding conditions of a rock mass considered as an equivalent continuum, a 3-D strength criterion is needed. It has been usual to use the well-established Mohr-Coulomb and Drucker-Prager criteria which define simple yield surfaces (pyramidal

surface and cone respectively) in the stress space. For rocks, a well-known criterion often used to account for the strength of intact rock as jointed masses is the Hoek-Brown criterion.

3-D Hoek and Brown Yield Surface

The original form of Hoek-Brown [9] criterion in terms of principal stresses is given by

$$\sigma_1 = \sigma_3 + \sqrt{m\sigma_c\sigma_3 + s\sigma_c^2}, \tag{14}$$

in which σ_1, σ_3 are the major and minor principal stresses at failure. The uniaxial strength is related to the parameter σ_c, while m, s are empirical parameters which describe the extent of breakage of the rock mass. The yield surface can be readily expanded under isotropic conditions and formulated in terms of principal invariants of the stress tensor, i.e.

$$F_{HB} = 4J_2\cos^2\theta + m\sigma_c\sqrt{J_2}\left(\frac{\sin\theta}{\sqrt{3}} + \cos\theta\right) + m\sigma_c\frac{I_1}{3} - s\sigma_c^2 = 0,$$
$$\sin 3\theta = -\frac{3\sqrt{3}}{2}\frac{J_3}{J_2^{3/2}}; \tag{15}$$

where I_1 is the first stress invariant, J_2 is the second deviatoric stress invariant, and θ the Lode angle related to the third deviatoric stress invariant J_3. This represents a curved pointed bullet with 6 curved parabolic surfaces in the octahedral plane, see Fig. 1. Unfortunately, singularities similar to Mohr-Coulomb arise at the intersection points, and these are not desirable when computing the gradient to the surface. However, the trace of the surface in the deviatoric plane can be smoothened out; for example Pan et al. [10] adopted a circular section for simplicity. In this study, a special smoothening technique which accounts for the representation of variable strengths in the stress space is derived.

Continuous 3-D Hoek and Brown Yield Surface

The failure surface is smoothened in such a way that its trace in the deviatoric plane is continuous and has continuous derivatives. This smoothness, or continuity condition is very important to ensure the gradient is unique. Also, from a computational point of view it is convenient to have a single description of the failure surface within the stress space. Since isotropic conditions prevail in the present context, only a sextant of the stress space need to

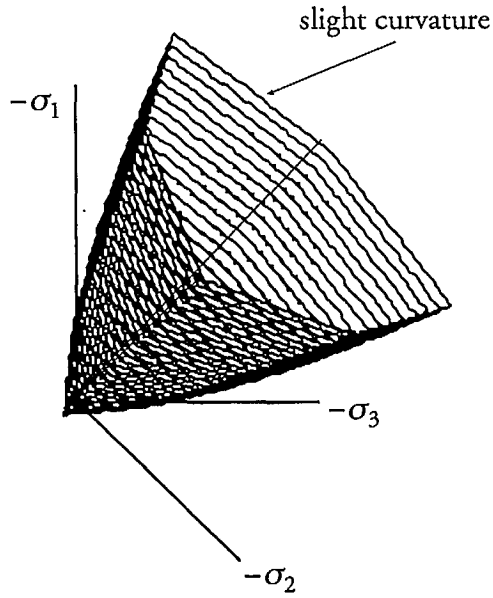

(a) principal stress view

Hoek and Brown parameters

$\sigma_c = 10MPa$

$m = 2.4$

$s = 0.082$

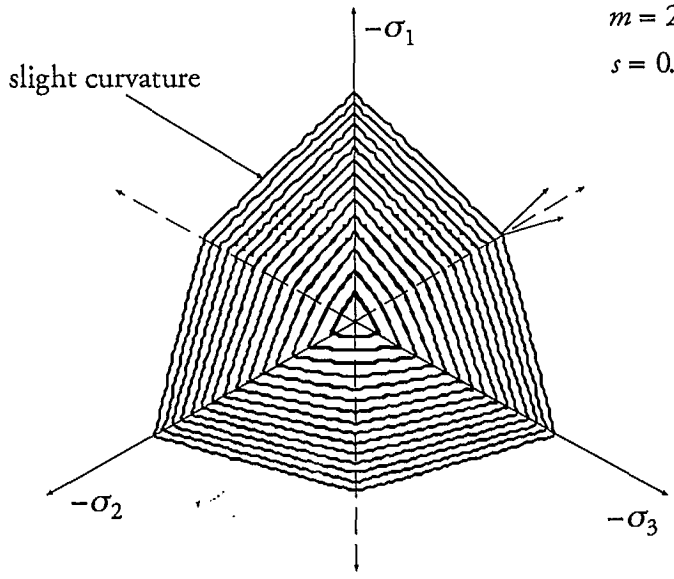

(b) deviatoric view

Figure 1. Generalized 3-D Hoek-Brown failure surface

be examined, i.e. $-\pi/6 \le \theta \le \pi/6$. An elliptic approximation is used to describe the variation of the trace of the failure surface in the deviatoric plane, as illustrated in Fig. 2.

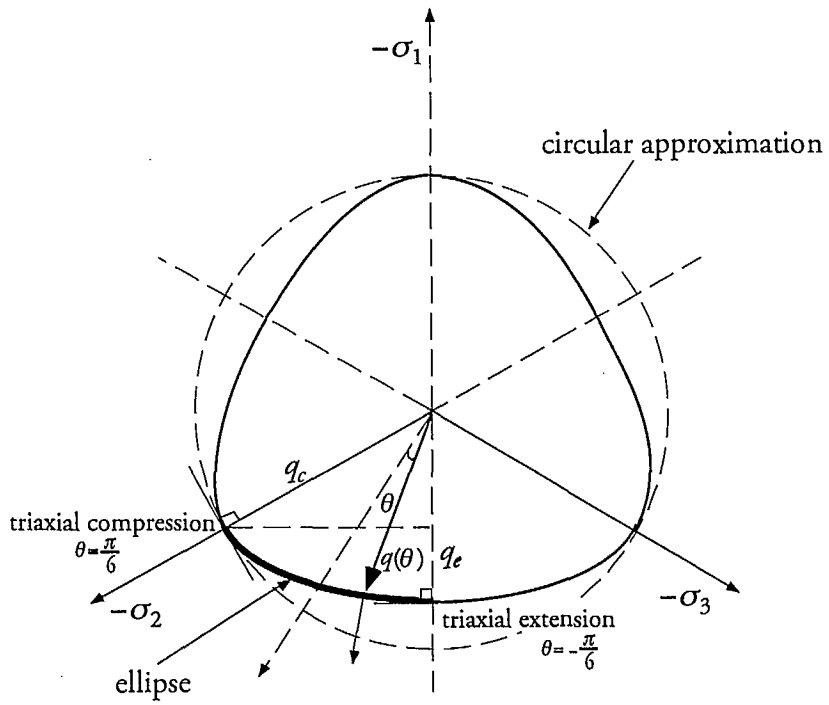

Figure 2. Elliptical approximation of deviatoric trace

The elliptic trace can be readily expressed in terms of polar coordinates via the following functional:

$$g(\theta) = \frac{4(1-e^2)\cos^2(\pi/6+\theta) + (1-2e)^2}{2(1-e^2)\cos(\pi/6+\theta) + (2e-1)\sqrt{4(1-e^2)\cos^2(\pi/6+\theta) + 5e^2 - 4e}}, \quad (16)$$

The eccentricity e defines the ratio of the deviatoric stress q in the extension branch to the one in the compression branch, i.e.

$$e = \frac{q_e}{q_c}. \quad (17)$$

In order to ensure smoothness and convex conditions, $0.5 < e < 1$ for the eccentricity e. As a result of using the functional g, a conical surface with curved meridian and smooth deviatoric trace is obtained with the space diagonal as axis of revolution, see Fig. 3. The mathematical

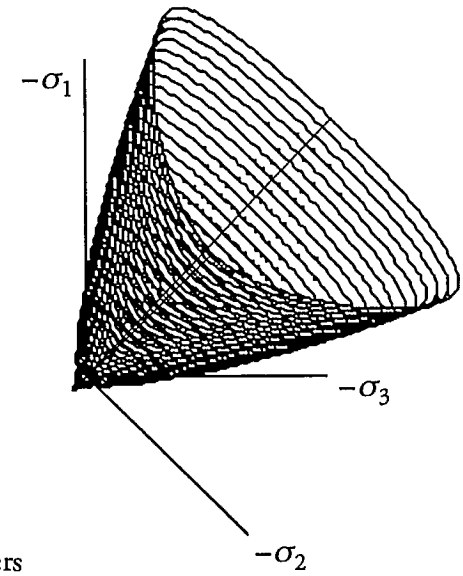

(a) principal stress view

Hoek and Brown parameters

$\sigma_c = 10MPa$

$m = 2.4$

$s = 0.082$

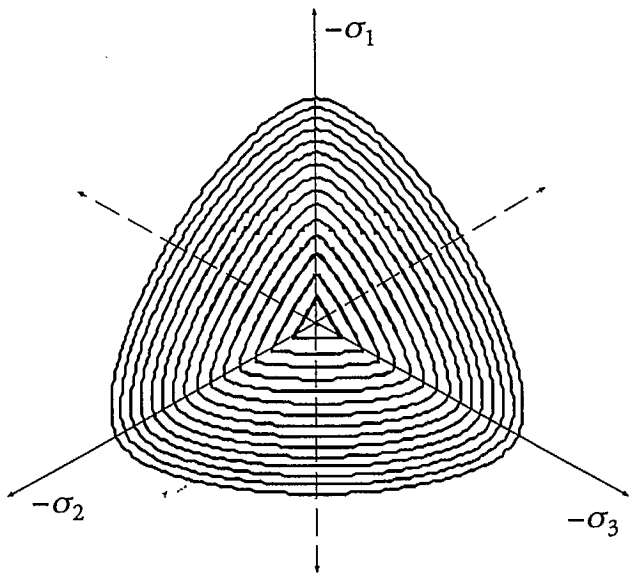

(b) deviatoric view

Figure 3. Smoothed 3-D Hoek-Brown failure surface

expression of the smooth, continuous 3-D Hoek-Brown surface as an extension to Eq. 15 is finally given by:

$$F(\boldsymbol{\sigma}) = q^2 g^2(\theta) + \sigma_c^* q\, g(\theta) + 3\sigma_c^* p - s\sigma_c^2 = 0;$$
$$\sigma_c^* = m\frac{\sigma_c}{3} \quad ; \quad q = \sqrt{3J_2} \quad \text{and } p = \frac{I_1}{3}. \tag{18}$$

Plastic Potential

It has long been recognized that an associated flow rule over-estimates the degree of plastic dilation and thus plastic work dissipation. In order to rectify and thus overcome this shortcoming, a plastic potential must be used in conjunction with the Hoek-Brown yield surface. Considering that a smooth and simple surface is desirable for computational reasons, the following form of plastic potential has been retained:

$$Q(\boldsymbol{\sigma}) = q^2 + n\sigma_c^{**} q + 3\sigma_c^{**} p; \quad \sigma_c^{**} = m^* \frac{\sigma_c}{3}. \tag{19}$$

The parameter m^* corresponds to a dilation coefficient while n determines the size of the deviatoric trace. Values of n=1 and 2 would correspond to a circular generalization of the deviatoric trace based on the triaxial compression and extension branches respectively. It is noted that when m^* equals m, an associated flow rule can be achieved provided n is properly adjusted. In contrast, plastic flow with no dilation takes place when m^* equals zero, in which case Eq. (19) degenerates into a generalized von-Mises type of surface.

STRESS RETURN

As seen further back, the stress integration scheme can be regarded as a return mapping operation of the general form:

$$\boldsymbol{\sigma}_{n+1}^{k+1} = \boldsymbol{\sigma}_{n+1}^{tr} - \Delta\lambda_{n+1}^{k} \mathbf{C}^e : \partial_{\boldsymbol{\sigma}} Q_{n+1}^{k}. \tag{20}$$

The stress return onto the yield surface follows a direction prescribed by the plastic potential Q. Fig. 4 geometrically illustrates the mechanics of the stress return in the p-q space and deviatoric plane. In the present context, due to the simple form of the plastic potential, the direction of plastic flow is radial in the deviatoric plane but not in a meridional section as

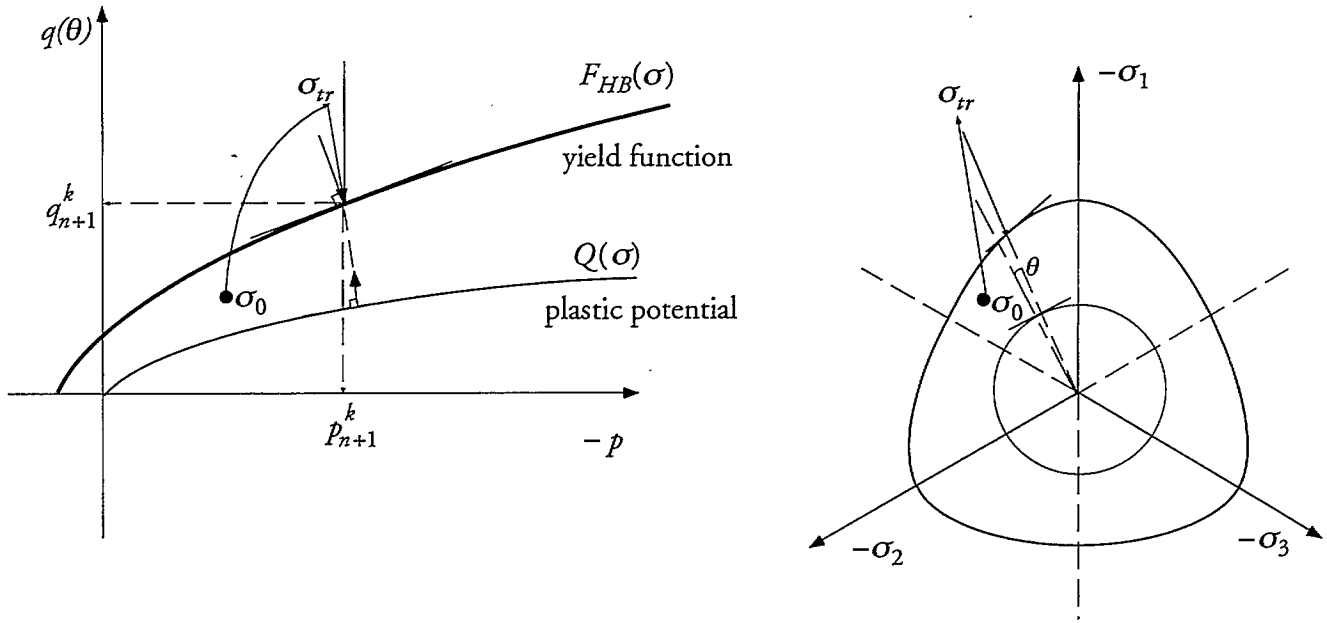

Figure 4. Stress return based on plastic potential Q

shown in the p-q space. The key observation is that when $F=Q$, the projection becomes indeed the closest point return and plastic flow is associated.

The isotropic elastic tensor C^{e} is classically given in terms of bulk modulus K and shear modulus G, i.e.

$$\begin{aligned} &\mathrm{C}^{e} = K\mathbf{1}\otimes\mathbf{1} + 2G(\mathrm{I} - \tfrac{1}{3}\mathbf{1}\otimes\mathbf{1}), \otimes = \text{tensor product}, \\ &\mathrm{I}_{ijkl} = \tfrac{1}{2}(1_{ik}1_{jl} + 1_{il}1_{jk}),\ 1_{ij} = \text{Kronecker delta}, \end{aligned} \tag{21}$$

Using the chain rule to evaluate $\partial_{\sigma} Q^{k}_{n+1}$ in terms of derivatives in p and q, and invoking Eq. (19), the term $\mathrm{C}^{e}:\partial_{\sigma} Q^{k}_{n+1}$ specializes into

$$\mathrm{C}^{e}:\partial_{\sigma} Q^{k}_{n+1} = K\frac{\partial Q^{k}_{n+1}}{\partial p^{k}_{n+1}}\ \mathbf{1} + \frac{3G}{q^{k}_{n+1}}\frac{\partial Q^{k}_{n+1}}{\partial q^{k}_{n+1}}\ s. \tag{22}$$

The above represents the stress return in terms of mean and deviatoric components whose directions are given by tensors $\mathbf{1}$ and s respectively. Herein, deviatoric stress is classically defined as $s = \boldsymbol{\sigma} - p\,\mathbf{1}$. Finally, substituting in for actual expressions of the gradient to the potential function Q, the stress return equation becomes

$$\boldsymbol{\sigma}^{k}_{n+1} = \boldsymbol{\sigma}^{tr}_{n+1} - 3K\sigma^{**}_{c}\Delta\lambda^{k}_{n+1}\ \mathbf{1} - \sqrt{6}G(2q^{k}_{n+1} + n\sigma^{**}_{c})\Delta\lambda^{k}_{n+1}\frac{s^{k}_{n+1}}{\left\|s^{k}_{n+1}\right\|}. \tag{23}$$

For convenience in the mathematics, the above stress return equation is written in terms of mean and deviatoric components as

$$p^{k}_{n+1} = p^{tr}_{n+1} - 3K\sigma^{**}_{c}\Delta\lambda^{k}_{n+1}, \tag{24}$$

$$s^{k}_{n+1} = s^{tr}_{n+1} - \sqrt{6}G(2q^{k}_{n+1} + n\sigma^{**}_{c})\Delta\lambda^{k}_{n+1}\frac{s^{k}_{n+1}}{\left\|s^{k}_{n+1}\right\|}. \tag{25}$$

Due to the radial nature of the stress return in the deviatoric plane (not in the meridional plane), the final and trial normalized stress vectors are co-linear in a direction defined by the radial unit tensor $\hat{n}$,

$$\hat{n} = \frac{s^{k}_{n+1}}{\left\|s^{k}_{n+1}\right\|} = \frac{s^{tr}_{n+1}}{\left\|s^{tr}_{n+1}\right\|}. \tag{26}$$

Also, taking the Euclidean norm of the final deviatoric stress in Eq. 25, and after some algebraic manipulations, one gets:

$$\left\| s_{n+1}^{k} \right\| = \left\| s_{n+1}^{tr} \right\| - \sqrt{6}\, G(2q_{n+1}^{k} + n\sigma_c^{**})\Delta\lambda_{n+1}^{k}. \tag{27}$$

Knowing that $q = \sqrt{\frac{3}{2}}\|s\|$, and rearranging terms in Eq. (27) finally yields the stress return for the deviatoric component,

$$q_{n+1}^{k} = \frac{q_{n+1}^{tr} - 3Gn\Delta\lambda_{n+1}^{k}\sigma_c^{**}}{(1 + 6G\Delta\lambda_{n+1}^{k})}. \tag{28}$$

Determination of Scalar Plastic Multiplier $\Delta\lambda_{n+1}^{k}$

The scalar value of the plastic multiplier $\Delta\lambda_{n+1}^{k}$ is obtained by merely imposing consistency requirement to Eq. 18a. At the k th. iteration,

$$F(\Delta\lambda_{n+1}^{k}) = \left[q_{n+1}^{k} g_{n+1}^{k}(\theta)\right]^2 + \sigma_c^{*} q_{n+1}^{k} g_{n+1}^{k}(\theta) + 3\sigma_c^{*} p_{n+1}^{k} - s\sigma_c^{2} = 0. \tag{29}$$

Furthermore, it is noted that the functional g which appears in the consistency condition in Eq. 29 depends on the Lode angle θ and the eccentricity e. Since the stress return is radial in the deviatoric space, the Lode angle remains unchanged during the geometrical projection. However, the final stress point may fall onto a point which belongs to a different deviatoric plane surface with a new value of mean pressure p. The eccentricity e will invariably change accordingly since it depends on the mean pressure through the following relation:

$$e = \frac{\sqrt{(\sigma_c^{*})^2 + (s\sigma_c^{2} - 3\sigma_c^{*} p)} - \sigma_c^{*}}{\sqrt{(\sigma_c^{*}/2)^2 + (s\sigma_c^{2} - 3\sigma_c^{*} p)} - \sigma_c^{*}/2}. \tag{30}$$

It is of interest to note that the above was obtained by invoking the definition in Eq. 17 and by replacing θ values of $-\pi/6$ and $\pi/6$ into the original Eq. 15 to calculate the deviatoric stress invariant in compression and extension respectively. Since the resulting consistency equation in Eq. (29) is non-linear in nature, solving for $\Delta\lambda_{n+1}^{k}$ requires a local Newton iteration with $\Delta\lambda_{n+1}^{0} = 0$ as initial estimate, and keeping θ constant. The algorithmic procedure is explicited in Box. 1.

Keeping Lode angle θ constant:

1. Initialize $k = 0$; $\Delta\lambda_{n+1}^{k} = 0$
2. Compute $F^{k} = F(\Delta\lambda_{n+1}^{k})$
3. If $\left|F^{k}\right| < \text{FTOL}$, exit; else
4. $\Delta\lambda_{n+1}^{k+1} = \Delta\lambda_{n+1}^{k} - F^{k} / F'(\Delta\lambda_{n+1}^{k})$
5. $k \leftarrow k+1$ and go to 2

Box. 1 Local Newton Raphson to determine plastic multiplier

The derivative of F with respect to $\Delta\lambda_{n+1}^{k}$ is readily obtained by chain differentiating Eq. 29. Note that the super- and sub-scripts which refer to the load and iteration steps will be temporarily dropped for sake of neatness of presentation. Accordingly, the derivative of F is given by

$$F'(\Delta\lambda_{n+1}^{k}) = 3\sigma_c^{*} p' + \left[2qg^{2}(\theta) + \sigma_c^{*} g(\theta)\right] q' + \left[2q^{2} g(\theta) + \sigma_c^{*} q\right] g'. \tag{31}$$

with

$$\begin{aligned} p' &= -3K\sigma_c^{**}, \\ q' &= -\frac{3G(2q + n\sigma_c^{**})}{(1 + 6G\Delta\lambda)}, \\ g' &= -\frac{\partial g}{\partial p} 3K\sigma_c^{**}. \end{aligned} \tag{32}$$

CONSISTENT TANGENT MODULUS

The generic expression for the final stress $\boldsymbol{\sigma}_{n+1}^{k}$ can be classically written in terms of mean and deviatoric parts as follows:

$$\boldsymbol{\sigma}_{n+1}^{k} = p_{n+1}^{k}\mathbf{1} + \sqrt{\frac{2}{3}}\, q_{n+1}^{k}\hat{\mathbf{n}}; \quad \hat{\mathbf{n}} = \frac{\mathbf{s}_{n+1}^{tr}}{\left\|\mathbf{s}_{n+1}^{tr}\right\|}. \tag{33}$$

With the preceding definition as seen far back in Eq. 13b., the consistent modulus is obtained by chain differentiating the stress tensor $\boldsymbol{\sigma}_{n+1}^{k}$ with respect to the final strain $\boldsymbol{\varepsilon}_{n+1}^{k}$ to lead to the following:

$$\mathbf{C}^{k}_{n+1} = \frac{\partial \boldsymbol{\sigma}^{k}_{n+1}}{\partial \boldsymbol{\varepsilon}^{k}_{n+1}} = \mathbf{1} \otimes \frac{\partial p^{k}_{n+1}}{\partial \boldsymbol{\varepsilon}^{k}_{n+1}} + \sqrt{\frac{2}{3}}\, \hat{\mathbf{n}} \otimes \frac{\partial q^{k}_{n+1}}{\partial \boldsymbol{\varepsilon}^{k}_{n+1}} + \sqrt{\frac{2}{3}}\, q^{k}_{n+1} \otimes \frac{\partial \hat{\mathbf{n}}}{\partial \boldsymbol{\varepsilon}^{k}_{n+1}}. \tag{34}$$

It can be easily shown, see [4], that the variation of the unit normal $\hat{n}$ with the final strain $\boldsymbol{\varepsilon}^{k}_{n+1}$ is given by:

$$\frac{\partial \hat{n}}{\partial \boldsymbol{\varepsilon}^{k}_{n+1}} = \frac{2G}{\left\| s^{tr}_{n+1} \right\|} \left(\mathbf{I} - \tfrac{1}{3}\mathbf{1} \otimes \mathbf{1} - \hat{n} \otimes \hat{n} \right). \tag{35}$$

The derivation of the consistent modulus also requires the calculation of derivatives of the mean pressure and deviatoric stress invariant with respect to the final strains. Thus, with the aid of Eqs. 24 and 28, straight forward differentiation yields

$$\frac{\partial p^{k}_{n+1}}{\partial \boldsymbol{\varepsilon}^{k}_{n+1}} = K \left[1 - 3\sigma_c^{**} \frac{\partial \Delta\lambda^{k}_{n+1}}{\partial \boldsymbol{\varepsilon}^{k}_{n+1}} \right], \tag{36}$$

$$\frac{\partial q^{k}_{n+1}}{\partial \boldsymbol{\varepsilon}^{k}_{n+1}} = \sqrt{6}\, \overline{G} \left[\hat{n} - \sqrt{\frac{3}{2}} (2q^{k}_{n+1} + n\sigma_c^{**}) \frac{\partial \Delta\lambda^{k}_{n+1}}{\partial \boldsymbol{\varepsilon}^{k}_{n+1}} \right], \quad \overline{G} = \frac{G}{(1 + 6G\Delta\lambda^{k}_{n+1})}. \tag{37}$$

Calculation of $\partial \Delta\lambda^{k}_{n+1} / \partial \boldsymbol{\varepsilon}^{k}_{n+1}$

In order to compute the consistent tangent modulus associated with 3-D Hoek-Brown yield criterion, it remains to calculate the derivative $\partial \Delta\lambda^{k}_{n+1} / \partial \boldsymbol{\varepsilon}^{k}_{n+1}$ which appears in Eqs. 36 and 37. Differentiation of the consistency equation with respect to $\Delta\lambda^{k}_{n+1}$ and hence $\boldsymbol{\varepsilon}^{k}_{n+1}$ implies

$$dF(\Delta\lambda^{k'}_{n+1}) = \frac{\partial F}{\partial p^{k}_{n+1}} \frac{\partial p^{k}_{n+1}}{\partial \boldsymbol{\varepsilon}^{k}_{n+1}} + \frac{\partial F}{\partial q^{k}_{n+1}} \frac{\partial q^{k}_{n+1}}{\partial \boldsymbol{\varepsilon}^{k}_{n+1}} \equiv \mathbf{0}. \tag{38}$$

Inserting Eqs. 36 and 37 into the above consistency and after collecting terms result into

$$\frac{\partial \Delta\lambda^{k}_{n+1}}{\partial \boldsymbol{\varepsilon}^{k}_{n+1}} = \overline{\alpha}\, \hat{n} + \overline{\beta}\, \mathbf{1}, \tag{39}$$

in which

$$\overline{\alpha} = \frac{\sqrt{6}\,\overline{G}}{\overline{M}}\frac{\partial F}{\partial q^k_{n+1}};\ \overline{\beta} = \frac{K}{\overline{M}}\frac{\partial F}{\partial p^k_{n+1}};\ \overline{M} = 3\overline{G}\,(2q^k_{n+1} + n\sigma_c^{**})\frac{\partial F}{\partial q^k_{n+1}} + 3K\sigma_c^{**}\frac{\partial F}{\partial p^k_{n+1}}. \quad (40)$$

The explicit expressions of $\overline{\alpha}$ and $\overline{\beta}$ can be readily obtained by calculating the gradient of the yield function F given in Eq. 18,

$$\frac{\partial F}{\partial q^k_{n+1}} = \left[2q^k_{n+1}g^k_{n+1} + \sigma_c^*\right]g^k_{n+1}, \quad (41)$$

$$\frac{\partial F}{\partial p^k_{n+1}} = 3\sigma_c^* + \left[2q^k_{n+1}g^k_{n+1} + \sigma_c^*\right]q^k_{n+1}\frac{\partial g^k_{n+1}}{\partial p^k_{n+1}}. \quad (42)$$

Calculation of $\partial p^k_{n+1} / \partial \boldsymbol{\varepsilon}^k_{n+1}$ ***and*** $\partial q^k_{n+1} / \partial \boldsymbol{\varepsilon}^k_{n+1}$

The derivatives in Eqs. 36 and 37 can now be conveniently expressed using Eq. 39. Thus,

$$\frac{\partial p^k_{n+1}}{\partial \boldsymbol{\varepsilon}^k_{n+1}} = K(1 - 3\overline{\beta}\,\sigma_c^{**})\,\mathbf{1} - 3\overline{\alpha}\,K\sigma_c^{**}\,\hat{n}. \quad (43)$$

$$\frac{\partial q^k_{n+1}}{\partial \boldsymbol{\varepsilon}^k_{n+1}} = -3\overline{G}\,\overline{\beta}(2q^k_{n+1} + n\sigma_c^{**})\,\mathbf{1} + \overline{G}(\sqrt{6} - 3(2q^k_{n+1} + n\sigma_c^{**})\overline{\alpha})\,\hat{n}. \quad (44)$$

The final form of the consistent modulus, corresponding to associated and non-associated stress return on the 3-D Hoek-Brown yield surface, emerges when substituting Eqs. 35, 43 and 44 into the general expression in Eq. 34, thus

$$\mathbf{C}^k_{n+1} = K(1 - 3\overline{\beta}\,\sigma_c^{**})\,\mathbf{1}\otimes\mathbf{1} - 3\overline{\alpha}\,\sigma_c^{**}K\,\mathbf{1}\otimes\hat{n} - \sqrt{6}\,\overline{G}\,\overline{\beta}\,\eta_q^*\,\hat{n}\otimes\mathbf{1} + \left[2\overline{G}(1 - \overline{\lambda}\xi) - \sqrt{6}\,\overline{G}\overline{\alpha}\,\eta_q^*\right]\hat{n}\otimes\hat{n} + 2G\,\xi\,(\mathbf{I} - \tfrac{1}{3}\mathbf{1}\otimes\mathbf{1}). \quad (45)$$

with

$$\eta_q^* = 2q_{n+1}^k + n\sigma_c^{**}; \quad \bar{\lambda} = 1 + 6G\Delta\lambda_{n+1}^k; \quad \xi = \frac{\left\|s_{n+1}^k\right\|}{\left\|s_{n+1}^{tr}\right\|}. \tag{46}$$

The final closed-form expression for the consistent modulus is given in a very convenient form for computer implementation. It leads to a symmetrical or non-symmetrical tensor depending upon whether an associative or a non-associative flow rule is adopted. Furthermore, it is found that the consistent modulus is solely expressed in terms of elastic parameters G and K and plastic components characterized by a combination of the radial direction $\hat{\boldsymbol{n}}$ and the space diagonal direction $\mathbf{1}$.

For matter of comparison, the classical continuum tangent modulus $\mathbf{E}_{n+1}^k$ which refers to the one obtained from the continuum and not from the algorithmic equations is given:

$$\begin{aligned}\mathbf{E}_{n+1}^k = {} & K(1-3\beta\sigma_c^{**})\ \mathbf{1}\otimes\mathbf{1} \ - \ 3\alpha\,\sigma_c^{**}K \ \ \mathbf{1}\otimes\hat{\boldsymbol{n}} \ - \ \sqrt{6}\,G\beta\,\eta_q^*\ \hat{\boldsymbol{n}}\otimes\mathbf{1} \\ & - \ \sqrt{6}\,G\alpha\,\eta_q^*\,\hat{\boldsymbol{n}}\otimes\hat{\boldsymbol{n}} \ + \ 2G\,(\mathbf{I}-\tfrac{1}{3}\mathbf{1}\otimes\mathbf{1}).\end{aligned} \tag{47}$$

The variables α, β, M and G which appear in the above are the un-barred versions of those listed in Eq. 40. An interesting point is that both expressions (Eqs. 46 and 47) take up the same form except that the shear modulus G appears to be scaled down by factors $\bar{\lambda}$ and ξ. This can be interpreted as degradation of the elastic parameter due to plastification. In particular, $\bar{\lambda}$ becomes significantly larger than 1 while ξ less than 1 when the trial stress shoots far outside the yield surface, which is the case for large load steps. Hence the continuum and consistent tangent operators may differ significantly, and it is probably this discrepancy which is responsible for degradation of the convergence characteristics as shown in the numerical example given at the end of this paper. To conclude, the traditional form of the continuum tangent modulus will coincide with the consistent tangent modulus only for infinitesimal load increments when $\Delta\lambda_{n+1}^k \to 0$ and $\xi \to 1$ which result into $\alpha = \bar{\alpha}$, $\beta = \bar{\beta}$, $G = \bar{G}$ and $M = \bar{M}$.

Stress Return for Tensile Region of Stress Space

The stress return and consistent tangent modulus derived in previous sections are valid as long as the trial stress falls within the region where stresses are compressive. When the trial stress shoots far out in the tensile zone of the stress space, special provision must be made to the algorithm. A simple cut-off surface F_2 is herein introduced to limit tension to a value p_t.

Seen this way, the model algorithm will have 3 basic response modes: *elastic mode, failure envelope mode and tension cut-off mode.* Figure 5 illustrates the different possible modes and the corresponding stress return.

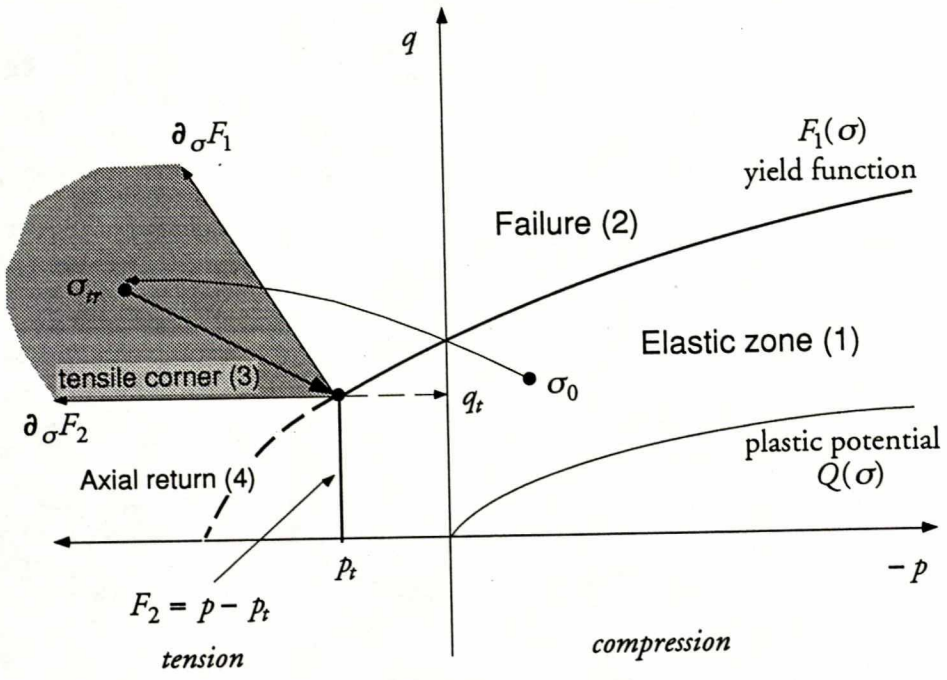

Figure 5. Stress return modes

The treatment of the tensile corner zone formed by the intersection of the Hoek-Brown failure and the tension cut-off surfaces demands particular attention since strict plastic consistency conditions must be satisfied. In such situation, both the failure surface and the tension cut-off are activated with the stress return taking place consistently and uniquely towards the vertex. The vertex point is determined on the basis of the Lode angle defined by the trial stress. This basically means that the stress is pulled back to the vertex formed by the intersection of the surfaces in the meridional plane containing the trial stress. Hence the vertex is given as

$$q \equiv q_t = \frac{1}{g(\theta_t, e_t)} \left\{ \sqrt{(\sigma_c^* / 2)^2 - 3\sigma_c^* p_t + s\sigma_c^2} \; - \; \sigma_c^* / 2 \right\}; \qquad p = p_t, \tag{48}$$

where the functional g is based on θ_t determined from the trial stress, and the eccentricity e_t of the trace of the failure surface in the tension cut-off plane. The stress return simply becomes $q_{n+1} = q_t$; $p_{n+1} = p_t$.

The consistent tangent modulus associated with such a stress return is readily obtained from Eq. 34. Due to the fixed nature of the vertex once the meridional section has defined,

the derivatives $\partial p^k_{n+1} / \partial \boldsymbol{\varepsilon}^k_{n+1}$ and $\partial q^k_{n+1} / \partial \boldsymbol{\varepsilon}^k_{n+1}$ which appear in Eq. 34 vanish. Hence, the compact form of the consistent modulus becomes

$$\mathbf{C}^k_{n+1} = \sqrt{\frac{2}{3}} q_t \frac{2G}{\|s^{tr}\|} (\mathbf{I} - \tfrac{1}{3}\mathbf{1}\otimes\mathbf{1} - \hat{\mathbf{n}}\otimes\hat{\mathbf{n}}). \tag{49}$$

In region 4, the trial stress is simply pulled in a direction parallel to the p axis, which is consistent with the vertical tension cut-off surface F_2. In this situation, the stress return equation and the consistent modulus are simply given by

$$\boldsymbol{\sigma}^k_{n+1} = s^{tr}_{n+1} + p_t\,\mathbf{1}; \quad \mathbf{C}^k_{n+1} = \frac{\partial s^k_{n+1}}{\partial \boldsymbol{\varepsilon}^k_{n+1}} = 2G(\mathbf{I} - \tfrac{1}{3}\mathbf{1}\otimes\mathbf{1}). \tag{50}$$

NUMERICAL TEST

The classical example of the excavation of a circular opening in an infinite homogeneous isotropic rock mass subjected to a uniform isotropic insitu stress σ_0 is considered. For constitutive behaviour, the rock mass is made to follow an elastic brittle-plastic material with yielding occurring whenever peak resistance is mobilized followed by a sharp drop in strength to residual values. The schematics of the problem geometry, its discretization and the material behaviour are given in Fig. 6.

The finite element mesh consists of 23 eight noded isoparametric elements with the radius of the external boundary 37 times the opening radius. The rock mass is made free to move in the radial direction but not in the longitudinal z direction due to the plane strain conditions prevailing in the infinitely long opening.

Associated Flow Rule

The Hoek and Brown parameters used in the analysis are E=10GPa, ν=0.25, σ_c=10 MPa, m^p=5, m^r= 1, s^p= 1, s^r = 0.1, where superscripts p and r stand for peak and residual. The inner wall pressure is initially subjected to the insitu stress value of the rock mass, i.e. 25 MPa. Excavation is simulated by releasing the internal pressure until it drops to zero in a stepwise manner. In order to investigate the effect of step size on the solution, the number of unloading steps to achieve zero internal wall pressure are made to be 5, 9 and 19 (large, medium and small).

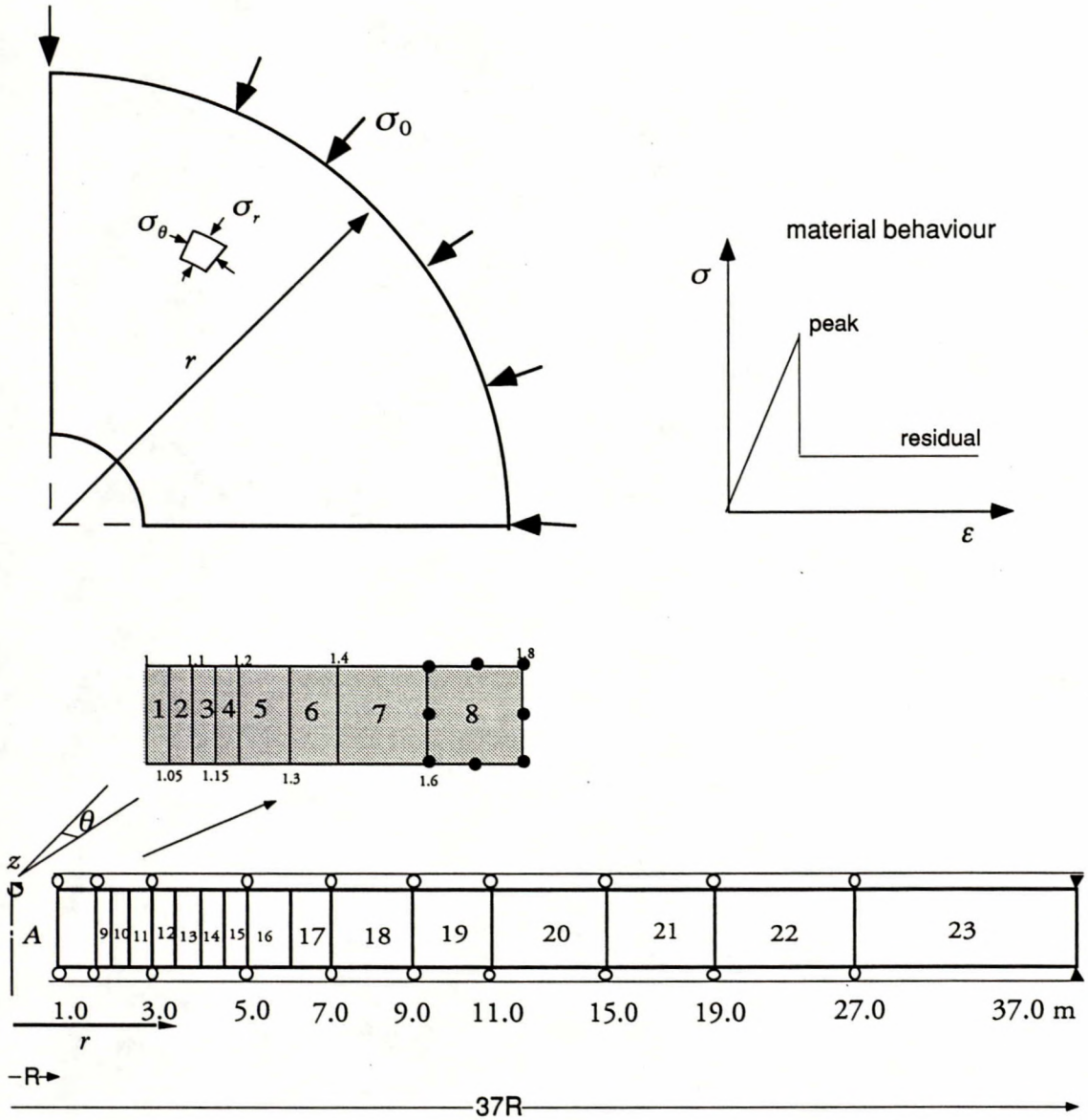

Figure 6. Discretized model for circular opening in infinite space

Figure 7a shows the distribution of radial, hoop and longitudinal stresses along the radius *r*. It is clearly seen that the solution is insensitive to unloading step size, whether the number of steps is 5, 9 or 19. The classical jump in stresses occurs at the boundary of the elastic and plastic regions for both the hoop and longitudinal stresses. In that particular case, the plastic radius is found to be about 3.6 m. The variation of displacement along the radial direction is given in Figure 7b and all three unloading schemes give basically the same distribution.

Table 1. gives the convergence characteristics of the consistent tangent modulus scheme as compared with the continuum formulation for the above problem. The superiority of the

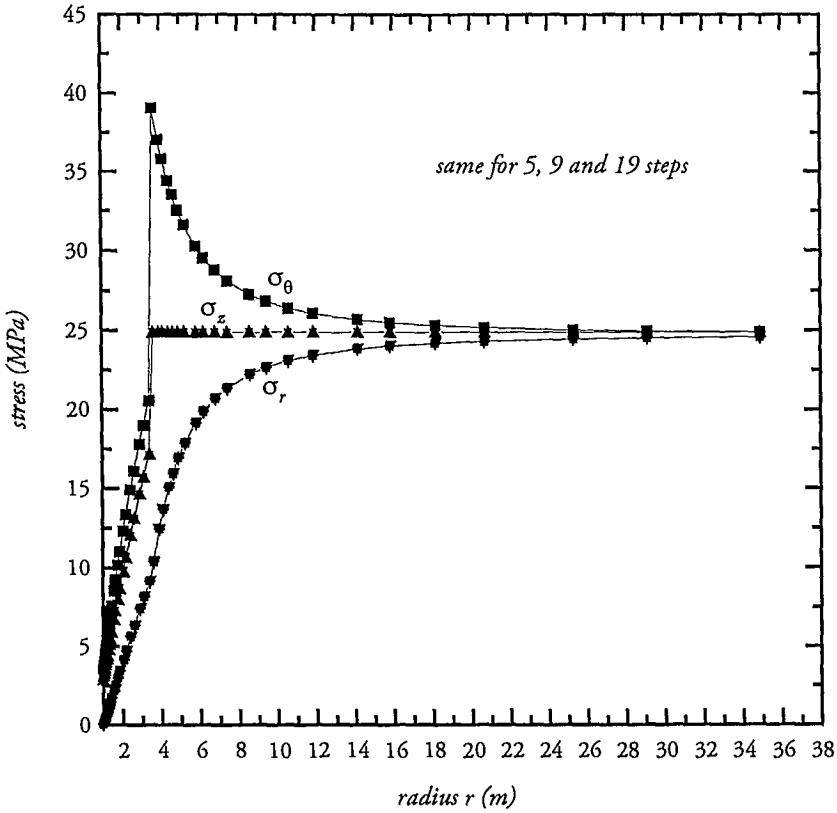

Figure 7a. Stress distribution along radial direction (associated flow)

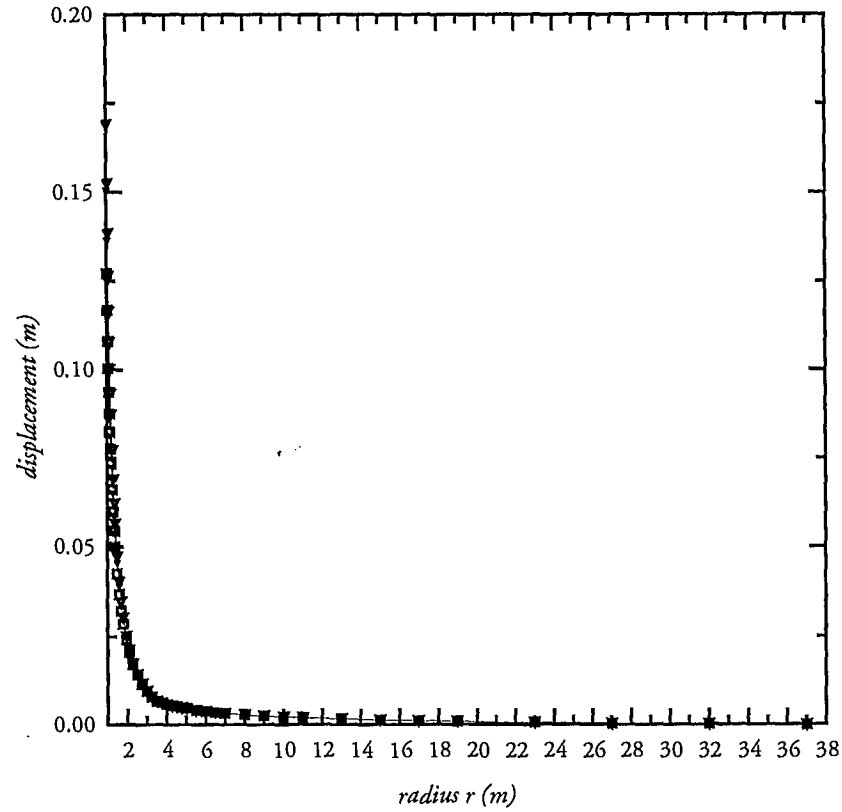

Figure 7b. Displacement profile along radial direction (associated flow)

consistent modulus approach is clear as plasticity becomes more pervasive towards the end of the unloading steps.

Table 1. Comparison of Convergency: Consistent vs. Continuum Tangent Modulus

		Consistent Tangent Modulus		Continuum Tangent Modulus	
LARGE: 5-step unloading scheme					
step no.	Load P	no. of iterations	force error	no. of iterations	force error
1	24.0	1	—	1	—
2	15.0	1	—	1	—
3	10.0	1	—	1	—
4	5.0	13	.9460E-07	>200	?
5	0.0	23	.1206E-06	>300	?
MEDIUM: 9-step unloading scheme					
1	24.0	1	—	1	—
2	20.0	1	—	1	—
3	15.0	1	—	1	—
4	10.0	1	—	1	—
5	8.0	11	.20602E-06	19	.6555E-05
6	6.0	10	.79410E-09	19	.8595E-05
7	4.0	13	.52380E-07	45	.1715E-04
8	2.0	14	.11690E-06	161	.2330E-04
9	0.0	23	.47010E-07	>300	?
SMALL: 19-step unloading scheme					
1	24.0	1	—	1	—
2	20.0	1	—	1	—
3	15.0	1	—	1	—
4	10.0	1	—	1	—
5	9.0	8	.2052E-06	15	.6665E-05
6	8.0	10	.2476E-06	17	.2225E-05
7	7.0	8	.3852E-06	15	.5700E-05
8	6.0	9	.8115E-09	16	.3110E-05
9	5.0	8	.2136E-09	22	.1100E-04
10	4.5	10	.7118E-07	19	.5100E-05
11	4.0	10	.1855E-06	21	.6660E-05
12	3.5	11	.8355E-07	29	.1188E-04
13	3.0	10	.1427E-06	18	.6929E-05
14	2.5	12	.2123E-06	43	.1478E-04
15	2.0	13	.3579E-06	72	.2148E-04
16	1.5	15	.1189E-06	100	.3902E-04
17	1.0	17	.5755E-07	>200	?
18	0.5	19	.3227E-06	>200	?
19	0.0	25	.3114E-06	>300	?

In particular, the case of large unloading in the 5-step scheme highlights the robustness achieved by the consistent tangent modulus formulation. The number of equilibrium

iterations needed when using the consistent tangent modulus were 13 and 23 for steps 4 and 5 respectively with force error of the order of 10^{-7}. The continuum tangent modulus method took over 300 iterations and the force error was larger. The same trend was found for the other unloading schemes when using the continuum formulation as convergence could not be achieved—or at least required an incredible number of iterates—for the last steps when the internal pressure became zero. Also, it is noticed that whenever convergence was achieved for the continuum tangent modulus, the force error was systematically larger than the one obtained using the consistent tangent modulus.

Non-Associated Flow Rule

The above problem was repeated using the plastic potential described in the previous sections for more adequate dilatancy via a non-associated flow rule. The parameter m^* which controls dilation was chosen to be 0.5. Note that in the previous study a value of 1.0 was used to achieve an approximately associated flow rule.

Figure 8a. shows the new stress distribution as compared with the one using an associated flow rule. As far as regard stresses, they were found to be identical, but as expected, the displacement profile gave a smaller convergence at the inner wall of the opening due to less dilation, see Fig. 8b. The number of equilibrium iterations needed were still within reasonable range. The most critical situation which involves the 5-step scheme was used. For the 4th. and 5th. unloading steps which correspond to an internal pressure of 5 and 0 MPa respectively, the number of iterations were 14 and 35 with force errors of the order of 10^{-6}. In contrast, the continuum tangent modulus scheme did not converge at all. It is found that in general, the degree of non-linearity increases in the non-associated case due to the more complicated direction of the stress return. However, this increase in level of difficulty does not seem to degrade very much the convergency characteristics of the scheme and thus confirms the robustness of the method.

Effect of Deviatoric Trace Curvature on Convergence

The case of a circular cross-section of the yield surface in the deviatoric plane was next tried by making the eccentricity e in the formulation to be equal to 1. Since the functional g in Eq. 16 reduces to unity, the expression of the yield surface given in Eq. 18 is simplified considerably and there is no longer dependence on the Lode angle θ, see [11]. In more precise terms the yield surface is derived from triaxial stress conditions and ignores the effect of the intermediate principal stresses.

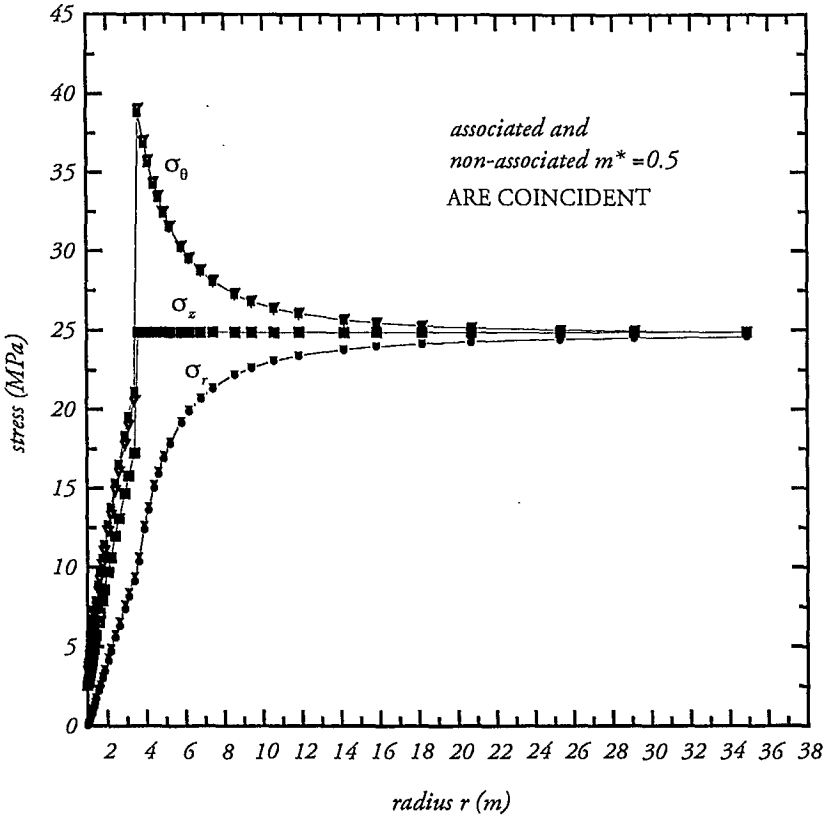

Figure 8a. Stress distribution along radial direction (non-associated flow)

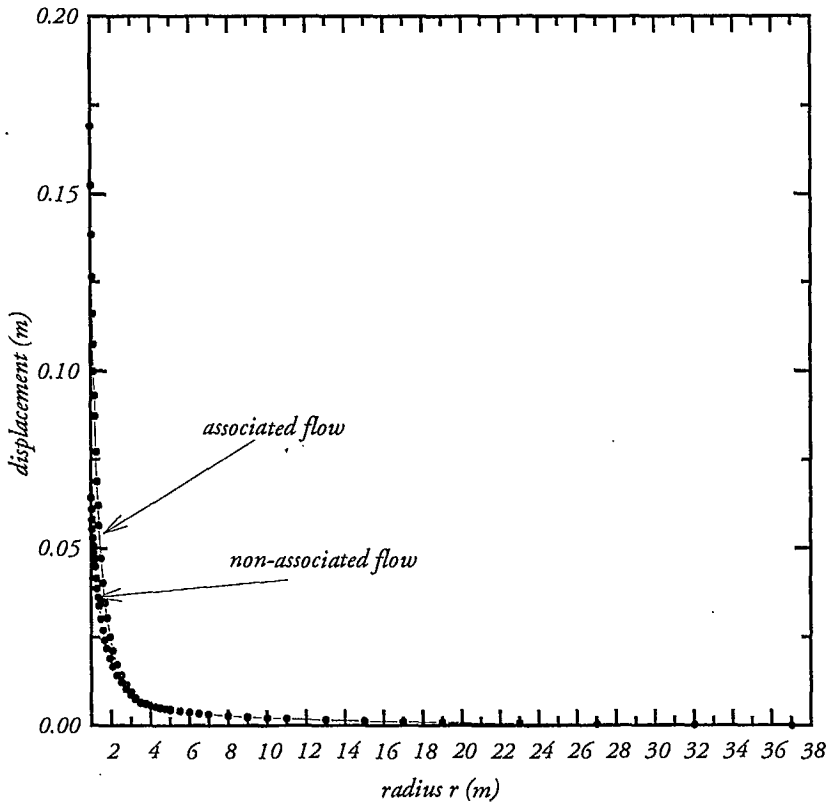

Figure 8b. Displacement profile along radial direction (non-associated flow)

Figure 9a illustrates the stress distribution obtained when using a circular approximation and comparison with results related to an elliptical smoothening. Note that the circular approximation is based on the triaxial compression branch which corresponds to a Lode angle of 30^0. It is found that the plastic radius obtained by using such approximation is smaller (2.4m instead of 3.6m) than the one obtained by the elliptical approximation. Also, the inner wall moves less, see Fig. 9b. The difference can be explained by the fact that the strength corresponding to the elliptical approximation is smaller as one moves between the triaxial compression and tension branches in the deviatoric plane. Therefore, a generalization based on parameters derived from the triaxial compression branch underestimates the extent of plasticity for a general stress situation such as the one met in plane strain conditions.

In terms of convergency rates, it is seen less number of iterations are needed for a circular approximation because of the simpler geometry of the yield function which involves a constant curvature; Fig. 10 depicts this observation. However, it is thought that for better representation of strength for states of stress other than triaxial, the level of complexity brought in by the elliptical approximation does not significantly degrade the convergency characteristics of the scheme; the number of iterations only increase by less than 2 fold in the case examined.

CONCLUSIONS

A consistent tangent modulus has been derived for the widely used Hoek-Brown failure criterion. The effect of the intermediate principal stress on yielding is accounted by a special 3-D stress generalization which yields a smooth deviatoric trace in the stress space by means of an elliptical functional. It is demonstrated that the implicit integration scheme in conjunction with a consistent tangent modulus ensures rapid convergence during the search for equilibrium in a non-linear finite element analysis. This is in contrast with the conventional so called continuum tangent moduli which tend to degrade the convergence rate as they are inconsistently calculated. The generic example of the excavation of a circular opening in an infinite rock mass demonstrates the effectiveness and robustness of the algorithm, especially when the load step becomes large. Also, equilibrium is satisfied rigorously since the error is in the order of 10^{-9}. It is seen that despite the level of complexity brought in by introducing an elliptical trace in the deviatoric plane and a plastic potential, the number of iterations still remain within permissible range (35 in the very extreme case as compared to over 300 when using the continuum tangent modulus). Also, the algorithm adopted in the super tension region can be effectively applied to a multi-surface model such as the cap model.

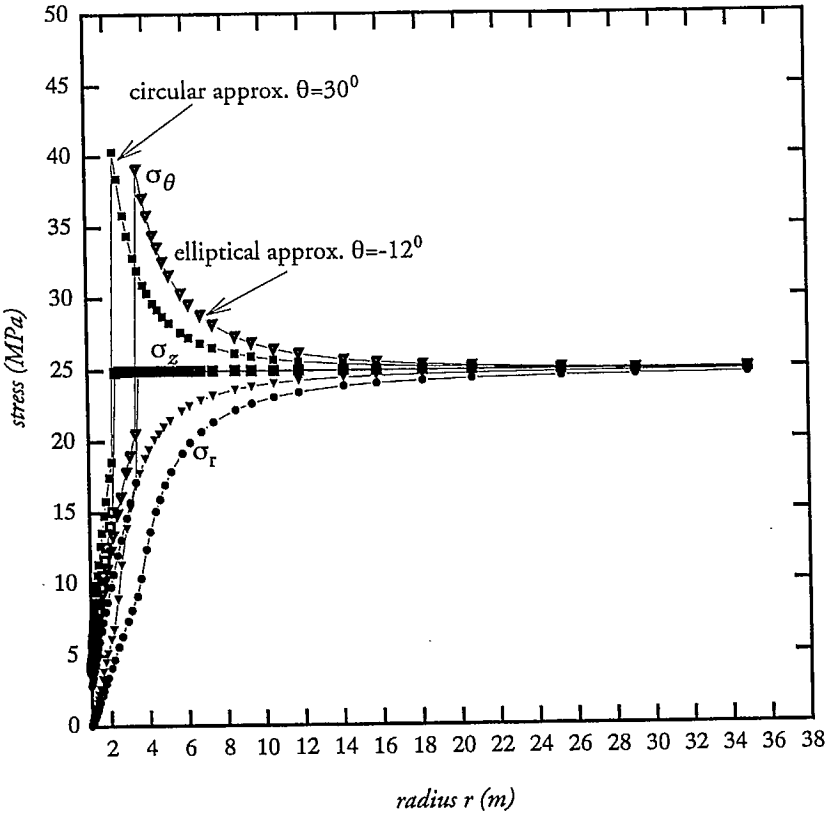

Figure 9a. Comparison of stress distributions: circular vs. elliptical approximation

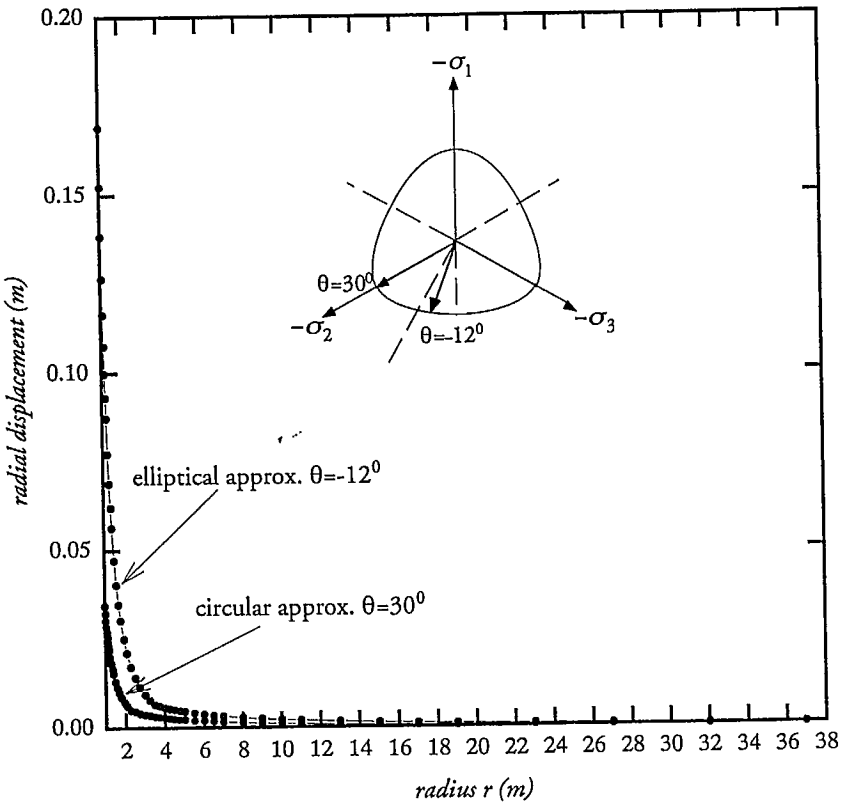

Figure 9b. Comparison of radial distributions: circular vs. elliptical approximation

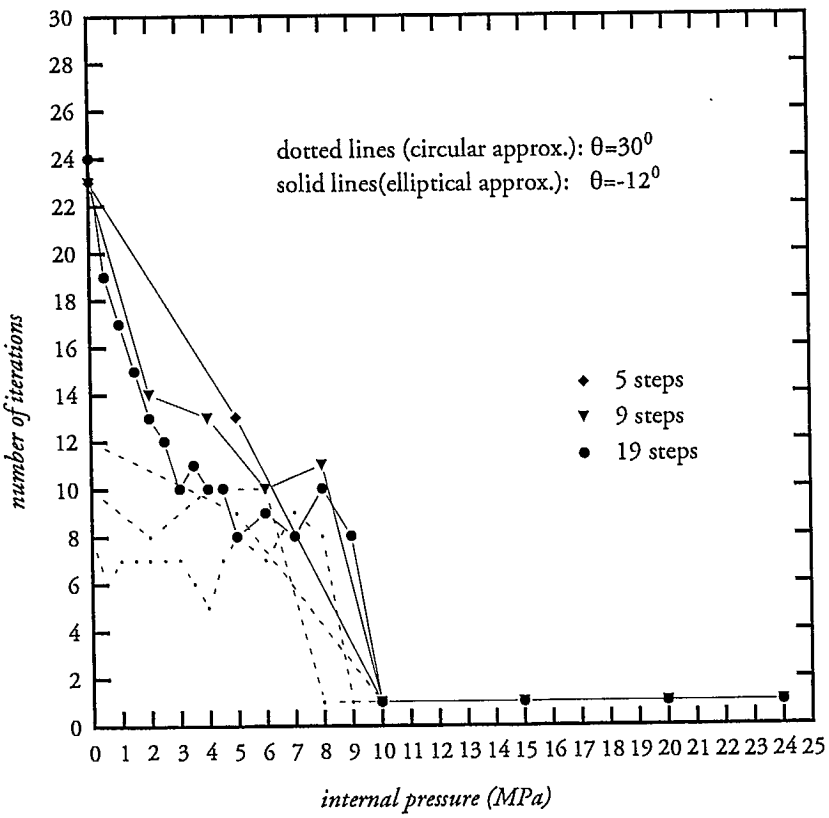

Figure 10. Comparisons of convergence rates for circular and elliptical approximations

ACKNOWLEDGEMENTS

The author wishes to express his gratitude to the Mining Research Laboratories of the Canadian Centre for Mineral and Energy Technology for providing support for this research.

REFERENCES

1. Owen, D.R.J and Hinton, E. Finite Elements in Plasticity, Pineridge Press, Swansea, UK, 1980.

2. Deng, X. and Rosakis, A. J. Negative Plastic Flow and its Prevention in Elasto-plastic Finite Element Computation, Finite Elements in Analysis and Design, Vol. 7, 2, (1990) 181-191.

3. Wilkins, M.L. Calculation of Plastic Flow, Methods of Computational Physics, Vol. 3, Academic Press, New York (1964).

4. Simo, J.C and Taylor, R.L. Consistent Tangent Operators for Rate-independent Elastoplasticity, Comp. Meth. Appl. Mech. Engr., Vol. 48, (1985) 101-118.

5. Ortiz, M. and Popov, E.P. Accuracy and Stability of Integration Algorithms for Elastoplastic Constitutive Relations, Int. J. Num. Meth. Engr., Vol. 21, (1985) 1561-1576.

6. Simo, J.C and Taylor, R.L. A Return Mapping Algorithm for Plane Stress Elastoplasticity, Int. J. Num. Meth. Engr., Vol. 22, (1986) 649-670.

7. Willam, K.J. Recent Issues in Computational Plasticity, Proceedings of the 2nd. International Conference on Computational Plasticity: Models, Softwares and Applications, Eds. D.R.J Owen, Hinton and Onate, Barcelona, Spain, (1989) 1353-1377.

8. Borja, R.I, Cam-Clay Plasticity, Part II: Implicit integration of constitutive equations based on non-linear elastic stress predictor. Computer Meth. in Applied Mech. and Eng. 88, (1991) 225-240.

9. Hoek, E. and Brown, E.T. Underground Excavations in Rock, London: Institution of Mining and Metallurgy , 1980.

10. Pan, X.D and Hudson, J.A. A Simplified Three Dimensional Hoek-Brown Yield Criterion, Rock Mechanics and Power Plants, Balkema, Rotterdam, (1988) 95-103.

11. Wan, R.G. A Consistent Return Algorithm for 3-D Hoek-Brown Failure Criterion, Numerical Models in Geomechanics (NUMOG IV), Swansea, Wales (1992) 619-628.